Journal of Alzheimer's Disease 71 (2019) 1125–1138
DOI 10.3233/JAD-190226
IOS Press

Intraneuronal Tau Misfolding Induced by Extracellular Amyloid-β Oligomers

Lauren K. Rudenko[a], Horst Wallrabe[a,b], Ammasi Periasamy[a,b], Karsten H. Siller[c], Zdenek Svindrych[d], Matthew E. Seward[a,e], Merci N. Best[a] and George S. Bloom[a,e,f,*]
[a]*Department of Biology, University of Virginia, Charlottesville, VA, USA*
[b]*W.M. Keck Center for Cellular Imaging, University of Virginia, Charlottesville, VA, USA*
[c]*Advanced Research Computing Services, University of Virginia, Charlottesville, VA, USA*
[d]*Department of Biochemistry and Cell Biology, Geisel School of Medicine, Dartmouth College, Hanover, NH, USA*
[e]*Department of Cell Biology, University of Virginia, Charlottesville, VA, USA*
[f]*Department of Neuroscience, University of Virginia, Charlottesville, VA, USA*

Handling Associate Editor: Alejandra Alonso

Accepted 31 July 2019

Abstract. Abnormal folding and aggregation of the microtubule-associated protein, tau, is a hallmark of several neurodegenerative disorders, including Alzheimer's disease (AD). Although normal tau is an intrinsically disordered protein, it does exhibit tertiary structure whereby the N- and C-termini are often in close proximity to each other and to the contiguous microtubule-binding repeat domains that extend C-terminally from the middle of the protein. Unfolding of this paperclip-like conformation might precede formation of toxic tau oligomers and filaments, like those found in AD brain. While there are many ways to monitor tau aggregation, methods to monitor changes in tau folding are not well established. Using full length human 2N4R tau doubly labeled with the Förster resonance energy transfer (FRET) compatible fluorescent proteins, Venus and Teal, on the N- and C-termini, respectively (Venus-Tau-Teal), intensity and lifetime FRET measurements were able to distinguish folded from unfolded tau in living cells independently of tau-tau intermolecular interactions. When expression was restricted to low levels in which tau-tau aggregation was minimized, Venus-Tau-Teal was sensitive to microtubule binding, phosphorylation, and pathogenic oligomers. Of particular interest is our finding that amyloid-β oligomers (AβOs) trigger Venus-Tau-Teal unfolding in cultured mouse neurons. We thus provide direct experimental evidence that AβOs convert normally folded tau into a conformation thought to predominate in toxic tau aggregates. This finding provides further evidence for a mechanistic connection between Aβ and tau at seminal stages of AD pathogenesis.

Keywords: Alzheimer's disease, amyloid-β, FRET, tauopathies, tau

INTRODUCTION

Misfolding and aggregation of the neuron-specific, axon-enriched, microtubule-associated protein, tau, is a hallmark of Alzheimer's disease (AD) and a spectrum of non-Alzheimer's tauopathies [1]. Under normal conditions, tau plays a role in promotion of microtubule assembly, stabilization of microtubules, and regulation of organelle trafficking along microtubules [2–4]. In AD, however, tau becomes hyperphosphorylated, binds microtubules less effectively, and aggregates into oligomers and filaments within neurons [5, 6]. While there are many ways to monitor tau oligomerization and filament formation, methods to monitor earlier conformational changes that may trigger tau aggregation are less developed. To address this issue, we developed a biosensor that detects tau misfolding in live cells.

*Correspondence to: George S. Bloom, Department of Biology, University of Virginia, PO Box 400328, Charlottesville, VA 22904-4328, USA. Tel.: +1 434 243 3543; E-mail: gsb4g@virginia.edu.

Tau contains several important structural domains that mediate its physiological roles, folding, and oligomerization. It has 0, 1, or 2 inserts of 29 amino acids each near its N-terminus, a proline-rich region with many potential phosphorylation sites located near the end of the N-terminal half of the protein, and 3 or 4 imperfect, tandem microtubule-binding repeat domains (MTBRs) of 31 or 32 amino acids each located in the C-terminal half [7, 8]. Interestingly, the second and third MTBRs are also responsible for tau-tau interactions in tau aggregates [9].

Monomeric tau is a natively unfolded protein. *In vitro*, it behaves like a random coil and does not spontaneously form filaments [10–12]. Abnormal tau aggregation into the straight and paired helical filaments characteristic of tauopathies is driven by a shift from random coil to a β-sheet structure of regions within the second and third repeat domains [13]. Even in its soluble monomeric state, tau is not entirely devoid of semi-stable structures. In solution, normal tau was shown to adopt a folded structure in which the N- and C-termini are close together with the C-terminal held closer to the MTBR. This configuration has been called the paperclip [14] or hairpin [15] conformation of tau.

There is evidence that tau assembly into filaments depends on an unfolding that abolishes that paperclip or hairpin structure. This form of tau is recognized by two conformation-dependent antibodies, Alz50 and MC-1, which label tau in early AD brain [16, 17]. Both antibodies recognize similar, but distinct discontinuous epitopes formed by short stretches of amino acids near the N-terminal and a region in the MTBR. Additional work has shown that both N- and C-terminal tau fragments inhibit full length tau polymerization into filaments [15, 18], supporting the model that a conformation change in which movement of the tau N- and C-termini away from each other is key to the conversion of normal tau into a toxic, misfolded form.

To test whether tau does, indeed, convert between folded and unfolded states in living cells, we developed and characterized a full-length tau biosensor labeled at its N- and C-termini with Venus and Teal fluorescent proteins, respectively (Venus-Tau-Teal). Because Teal and Venus constitute an effective donor-acceptor pair for Förster resonance energy transfer (FRET), Venus-Tau-Teal allowed us to visualize normally folded (paperclip/hairpin) and unfolded tau in live cells that expressed the biosensor. Venus-Tau-Teal is operationally analogous to a previously described FRET biosensor from another group based on 0N4R tau labeled with CFP and YFP [19]. A key distinction between the present study and the earlier publication is that our approach ensured that intramolecular FRET signals, an indicator of the conformation of individual tau molecules, was minimally contaminated by intermolecular FRET signals or FRET-inhibiting effects due to tau-tau aggregation.

By expressing Venus-Tau-Teal in CV-1 African green monkey kidney fibroblasts and primary mouse cortical neurons, we obtained evidence that microtubule-associated tau has a folded, paperclip/hairpin-like conformation that can be modulated by drugs affecting microtubule binding or tau phosphorylation. Most importantly, we found that amyloid-β oligomers (AβOs) cause tau to unfold and adopt a conformation associated with toxic tau aggregates. These observations provide direct evidence that AβOs control tau conformation, and thereby constitute yet another example of how Aβ and tau work together to drive AD pathogenesis [20].

MATERIALS AND METHODS

Cell culture

Cell culture reagents were from Gibco/Invitrogen unless specified otherwise. Primary cortical neurons were isolated from wild type (C57/Bl6) mouse embryos aged approximately 18 days as previously described [21, 22], except that phenol red-free Neurobasal medium was used exclusively. CV-1 African green monkey kidney cells (ATCC catalog # CCL-70) were maintained in Dulbeco's Modified Eagle's Medium (DMEM) with 10% fetal bovine serum and 50 μg/ml gentamycin, and were dissociated with TyrpLE Express (Thermo Fisher) for subculturing. For live imaging, CV-1 cells and neurons were plated onto 14 mm #1 glass-bottom MatTek dishes.

Fluorescent fusion proteins

Expression vectors for singly and doubly labeled tau are in the background vector pCSC-SP-PW-NepX (pBOB-NEPX; from Inder Verma, Addgene plasmid #12340). Human 2N4R tau coding sequence was inserted between the Age1 and HpaI restriction sites by standard restriction digest techniques. cDNAs for the fluorescent proteins, mTFP (Teal) [23] and Venus [24] were then inserted at the N-terminal Age1 site or the C-terminal HpaI site, and confirmed for sequence accuracy and direction of insertion. The expected spectral properties and sizes

of all fluorescent fusion proteins were confirmed by spectral imaging and western blots using mouse monoclonal Tau5 antibody [25]. Constructs were then inserted into lentivirus with the packaging vectors pMD2.G (from Didier Trono, Addgene plasmid #12259) and psPAX2 (from Didier Trono, Addgene plasmid #12260) using the lentiviral protocol provided by Thermo Fisher for Lipofectamine 3000 production of lentivirus (Thermo Fisher L3000015.)

Wild type neurons were transduced with lentivirus between day 8 and day 10 *in vitro*. CV-1 cells were infected at approximately 60% confluence to allow for easier imaging of individual cells. Expression was monitored until the fluorescence was visible on an EVOS FL microscope (ThermoFisher). Cells were ready for imaging approximately 2 days post-transduction for CV-1 cells and approximately 4 days for neurons.

Western blotting

Western blots for Supplementary Figure 1 were run using Bio-Rad 10% mini-PROTEAN pre-cast gels in Tris/Glycine SDS running buffer. Boiled samples were run alongside precision Plus Protein ladder (1610374). Staining for tau utilized mouse monoclonal Tau5 antibody [25] and mouse monoclonal anti-GFP (NeuroMab clone N86/38; also recognizes Venus) with secondary Licor antibodies: IRDye 800CW Donkey anti-rabbit IgG (926-32213) and IRDye 680RD Donkey anti-mouse IgG (926-68072). Protein phosphorylation relied on rabbit polyclonal anti-tau (pS262) (Anaspec AS-54973) and rabbit polyclonal anti-phosphoSerine/Threonine (Cell Signaling 9381) primary antibodies. Mouse monoclonal anti-tau oligomer antibodies were kindly provided by Dr. Nick Kanaan of Michigan State University (TOC1), and Rakez Kayed of the University of Texas Medical Branch at Galveston (TOMA-1, TTC-35, and TTC-99).

Imaging

For CV-1 cells, standard DMEM was replaced with phenol red-free DMEM prior to imaging. FRET imaging was done on a Zeiss 780 confocal/ NLO/FLIM microscope. Excitation for intensity FRET experiments used an Argon-ion laser (458 nm and 514 nm excitation; 455–500 nm and 526–579 emission). Confocal FRET images were acquired with a GaAsP (Gallium Arsenide Phosphide) detector with approximately 40% quantum efficiency. 2-photon FLIM-FRET images were acquired by exciting the donor (Teal) with a Coherent Chameleon Vision-II Ti:Sapphire laser tuned to 820 nm (Becker & Hickl, Germany). A time correlated single photon counting (TCSPC) board (SPC-150) was used with a high-sensitivity hybrid GaAsP detector (HPM-100–40, 300–650 nm). Images were acquired with a 40X oil objective (1.30 NA). All live imaging was done on a temperature-controlled stage at 37°C with humidified 5% CO_2/95% air gas flow to maintain pH and humidity.

Tau and Aβ oligomer preparation

Tau oligomers were prepared as described previously [22, 26]. 2N4R tau was brought to 4 μM in 100 mM Tris pH 7.4, 0.1 mM EDTA, and 150 μM Tris(2-carboxy-ethyl)phosphine (TCEP; Life Technologies) and treated overnight with 50 μM benzophenone-4-maleimide (B4M; Sigma-Aldrich) followed by 5 mM dithiothreitol (DTT; Roche) to inactivate B4M, and dialyzed into 100 mM Tris, 0.1 mM EDTA, and 5 mM DTT. A portion was removed and flash frozen for monomer treatments, and the remaining protein was aggregated overnight in the presence of 150 μM arachidonic acid. The oligomers were treated for 5 min with UV light at 254 nm (Spectroline model EF-180), then flash frozen in small aliquots to be used immediately after thawing.

Amyloid-β oligomers (AβOs) were prepared from lyophilized synthetic $A\beta_{1–42}$ (AnaSpec), dissolved in HFIP (1,1,1,3,3,3-hexafluoro-2-propanol; Sigma-Aldrich Co.) to 1 mM and evaporated overnight at room temperature. The dried powder was resuspended in DMSO to 5 mM and sonicated for 10 min in a water bath. The peptide was then diluted to 100 μM in Neurobasal media, and incubated for 48 h at 4°C with rocking. Prior to use, oligomers were spun briefly to remove large oligomers and fibrils, bringing the concentration in solution to approximately 50 μM.

Experimental perturbation of cells

Cells were imaged prior to any medium additions and then nocodazole, okadaic acid (OA) or taxol (all from Abcam), were added to a final concentration of 1 μM while the cultures remained in place on the microscope stage. One hour later, the same fields of view were imaged again.

Aβ and tau oligomer treatments were too long to be done on stage without compromising the health of the cells, so parallel coverslips were imaged for treated and control cultures for these conditions. For AβO treatments, neuron medium (Neurobasal + B27) was replaced with B27-free Neurobasal, and 1 h later freshly prepared AβOs (see above) were added to the medium to a final concentration of approximately 1.5 μM total Aβ. Cells were imaged 6 h later. For tau oligomer treatments, freshly thawed aliquots (see above) were diluted into medium to a final concentration of 250 nM total tau 18 h before imaging.

Thresholding for intramolecular FRET

Images were taken in parallel on the same system for intensity (confocal) FRET and 2-photon lifetime FRET (FLIM). It was determined that intensities below 750 arbitrary units of acceptor intensity had minimal contamination of intermolecular FRET (see Fig. 3 and corresponding text). Using the parallel images, we determined that this intensity range corresponded to a photon count of lower than approximately 500 on the 2-photon detector, so cells were selected to be primarily within this expression range. All images then had single pixel regions of interest selected above background (varied slightly by experiment; usually 30–50 photons) and below a photon count of 500. Doing so excluded any cells or regions of cells that had a biosensor concentration that might have yielded significant intermolecular FRET according to the analysis described in Fig. 3.

FRET/FLIM analysis

Intensity FRET analysis was done largely in ImageJ (https://imagej.nih.gov/ij/) via a PFRET plugin written at the University of Virginia's Keck Center for Cellular imaging. This plugin allows subtraction of background and removal of spectral bleedthrough. After these corrections the result is a calculated E% (efficiency of energy transfer) for each region of interest (ROI) [27, 28].

FLIM images were first analyzed by Becker & Hickl SPCImage software (https://www.becker-hickl.com/). Curve fitting procedures done as described previously [29, 30]. Briefly, an exponential decay curve was fitted such that the χ^2 was approximately 1 (with a two-component analysis of the donor, incomplete exponential decay, and a measured instrument response function). These data were exported in a series of asc files. 2-photon images were used to designate single pixel regions of interest within the previously determined intensity range. A Fiji (https://fiji.sc/) macro written by us was then used to measure pixel intensity values in the selected ROIs and generate Excel (Microsoft) based result files for each image, which included a calculated lifetime value for each pixel/ROI. Some additional manual filtering of the results to remove outliers was performed including any ROIs with a χ^2 below 0.5 or above 2.0 (indicating the ROI was not well fitted by the decay curve). Lifetimes below 500 ps were also disregarded. These very low lifetimes were often seen outside of cells in the background, associated with very large χ^2 values and were not in the reasonable range for the fluorophore (possibly due to dying cells or degraded biosensors). Lifetimes were plotted as a frequency distribution histogram to determine the peak and distribution of the lifetime for each image/condition.

For each Fig. (3–6), a single "experiment" constitutes 6–9 fields of view per condition, with 1-2 cells per field of view. The number of ROIs analyzed per field of view/experiment varied significantly based on how many were removed by threshholding (as background pixels, too bright, poor χ^2), but most fields of view were in the range of 5–10 thousand analyzed ROIs after thresholding.

Statistical analysis

GraphPad Prism 7 software was used to analyze each data set by Kolmogorov-Smirnov test or one-way analysis of variance with a Tukey *post-hoc* test or *t*-test as appropriate.

RESULTS

Teal and Venus were chosen as FRET donor and acceptor, respectively, because of their superior fluorescence properties compared to other fluorescent protein pairs with similar excitation and emission spectra [23, 24, 31]. When Venus and Teal are in close enough proximity to cause a FRET event (approximately 10 nm or less), energy transfer efficiency rises and donor fluorescence lifetime declines with decreasing distance between the fluorophores. To establish the optimal structure for a tau folding biosensor, we designed Venus-Tau-Teal, Teal-Tau-Venus, and four singly tagged fusion proteins: Venus-Tau, Teal-Tau, Tau-Venus, and Tau-Teal (Fig. 1). The singly tagged proteins were necessary for calculating spectral bleedthrough for intensity

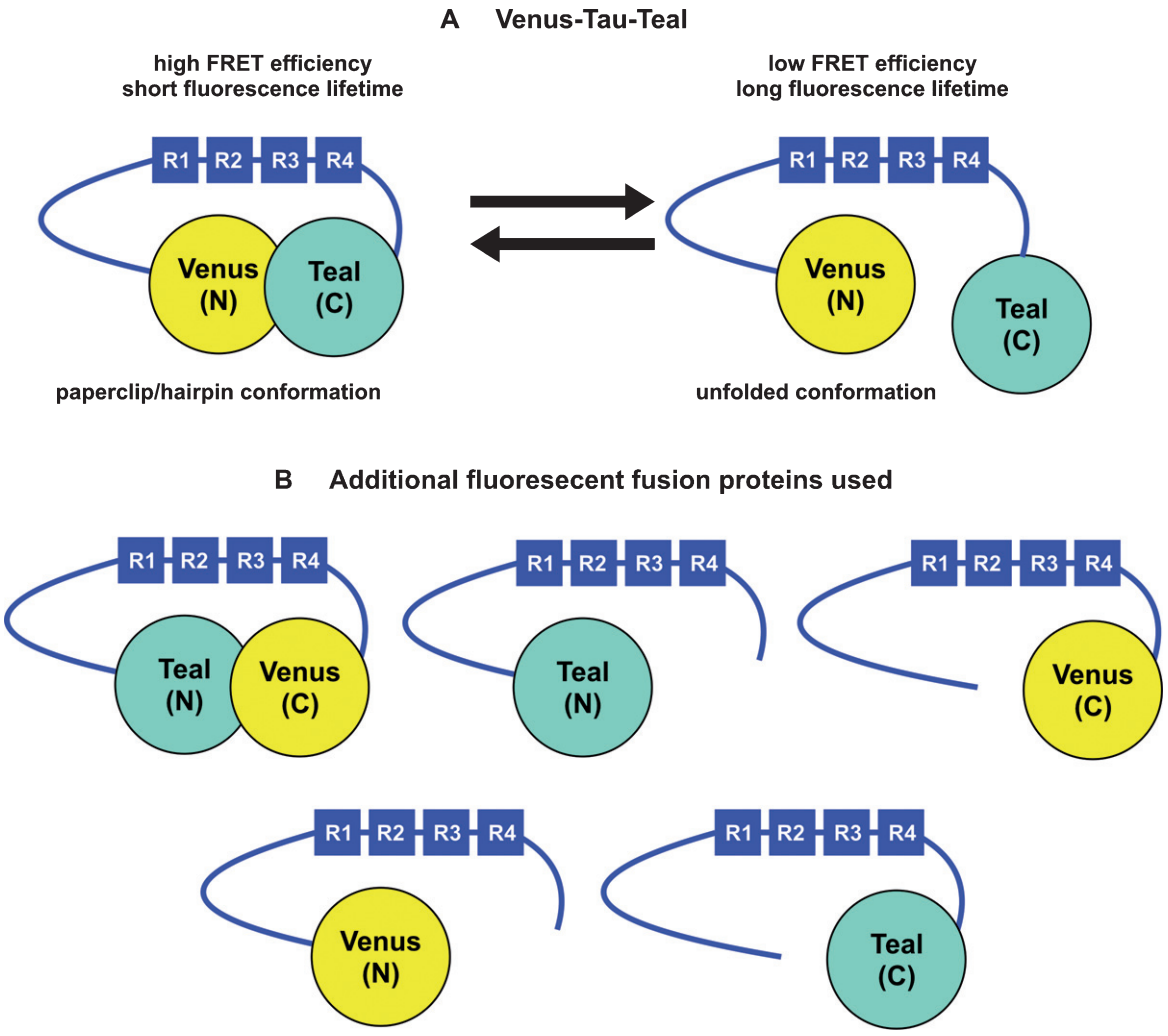

Fig. 1. Fluorescent tau fusion proteins. Illustrated here are the fluorescent fusion proteins of human 2N4R tau used in this study. A) Venus-Tau-Teal was compared with B) Teal-Tau-Venus for discriminating intramolecular from intermolecular FRET (see Fig. 3), and the singly labeled fluorescent fusion proteins in B) were used as standards for FRET efficiency (E%) and FLIM experiments. R1, R2, R3, and R4 signify the microtubule-binding repeat domains of tau.

FRET efficiency (E%) measurements [28] and the fluorescence lifetime of unquenched donor (Teal) for fluorescence lifetime imaging (FLIM) [31]. When expressed in CV-1 African green monkey kidney fibroblasts and imaged by confocal microscopy, all singly (Fig. 2) and doubly (Fig. 3) labeled fusion proteins localized to microtubules, indicating that coupling Teal, Venus, or both to tau does not obviously impair tau's microtubule-binding activity.

Teal-Tau-Venus and Venus-Tau-Teal are capable, in principle, of producing intramolecular FRET. In addition, each protein is theoretically capable of aggregating to form oligomers or filaments resulting in intermolecular FRET because of favorable orientations of Teal and Venus on adjacent fluorescent fusion proteins. Intermolecular FRET could also be generated by unfolding coupled with a parallel arrangement of individual fluorescent fusion proteins within aggregates. To use a doubly tagged protein as a FRET biosensor for the folding state of tau, we therefore had to identify conditions in which measured FRET signals are unaffected by fluorescent fusion protein aggregation. This was accomplished by analyzing Teal-Tau-Venus and Venus-Teal-Tau at various expression levels in CV-1 cells.

More specifically, we sought to establish an expression range in which FRET efficiency (E%) is independent of expression level and therefore is

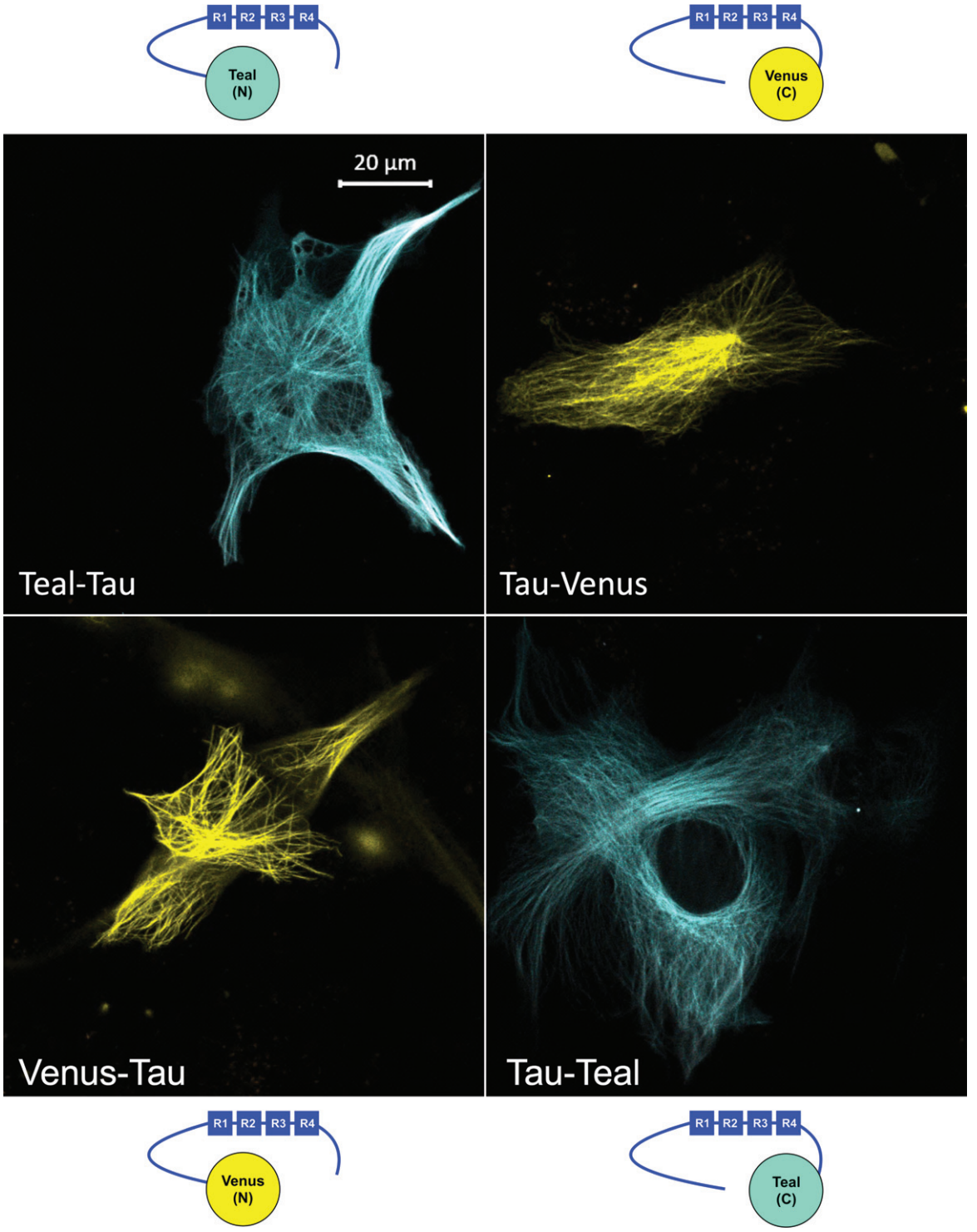

Fig. 2. Expression of singly labeled fluorescent tau fusion proteins in CV-1 fibroblasts. All such fluorescent fusion proteins target to microtubules. These proteins were used for subtracting spectral bleedthrough for FRET efficiency (E%) measurements and for calculation of unquenched donor (Teal) fluorescence lifetime for FLIM experiments.

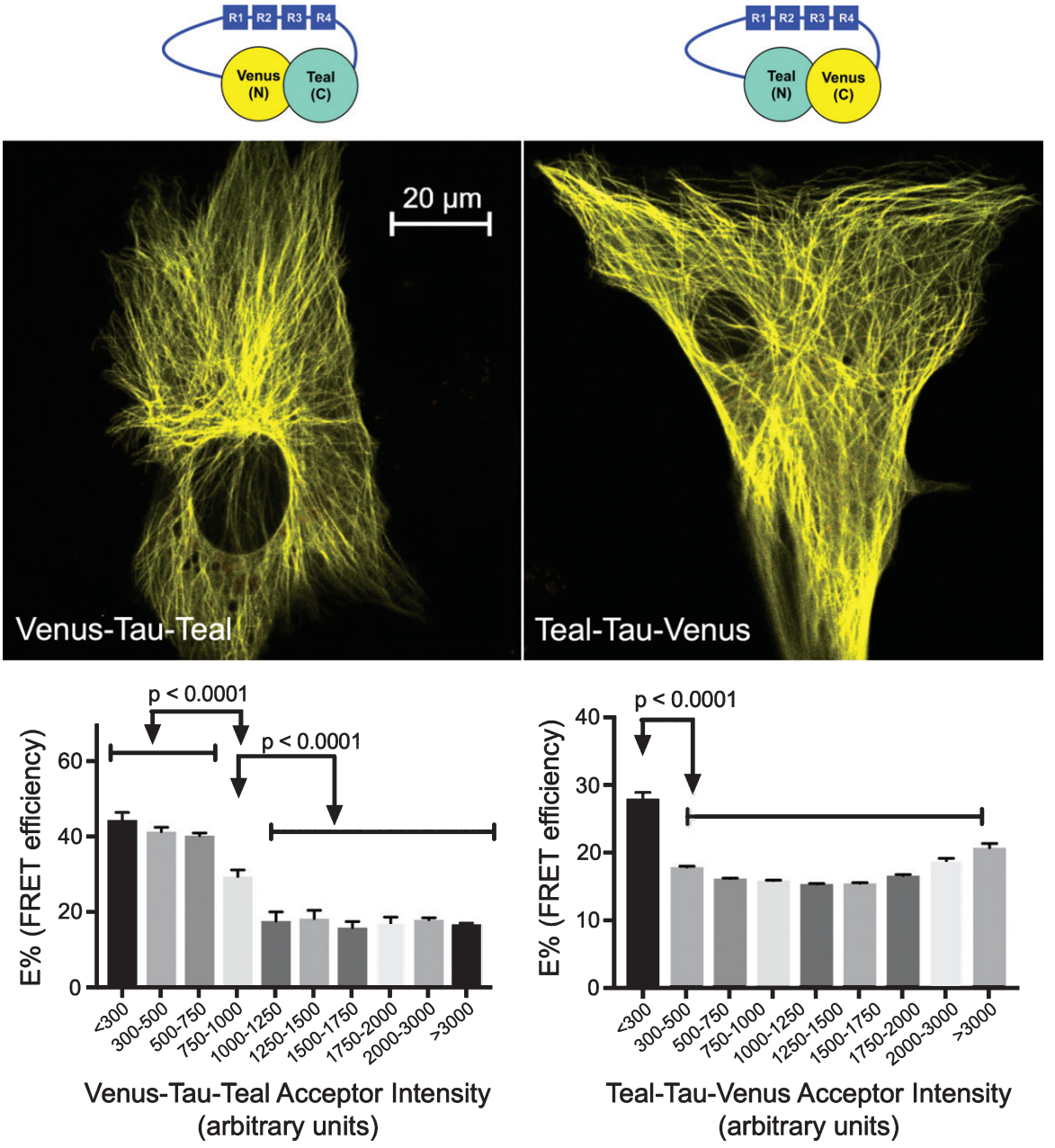

Fig. 3. Venus-Tau-Teal is superior to Teal-Tau-Venus for detecting intramolecular FRET uncompromised by aggregation effects. Venus-Tau-Teal and Teal-Tau-Venus both target to microtubules and show differing dependence of FRET efficiency (E%) on fluorescent fusion protein concentration. Venus-Tau-Teal, but not Teal-Tau-Venus, shows a broad range of E% independent of increasing acceptor (Venus) intensity (up to 750 arbitrary intensity units). FRET within that Venus intensity range was therefore judged to be predominantly intramolecular, and Venus-Tau-Teal was used as the tau conformation biosensor for all subsequent experiments. To minimize FRET signal contamination caused by Venus-Tau-Teal aggregation, we restricted subsequent observations to the low end of the range in which E% is independent of Venus intensity (correlated to a photon count of less than ~500 arbitrary intensity units). Bar graphs represent the merged data of 6 fields of view per experiment, repeated in four biological replicates with their standard errors of the mean. Statistical significance was determined by one-way ANOVA with Tukey's *post-hoc* test for multiple comparisons. Standard errors calculated by Prism column statistics.

dominated by intramolecular FRET. Since an intermolecular FRET signal would be dependent on the amount of biosensor expressed, a significant effect of acceptor intensity on calculated E% would indicate the FRET signal includes a substantial intermolecular component. Venus-Tau-Teal expression levels were

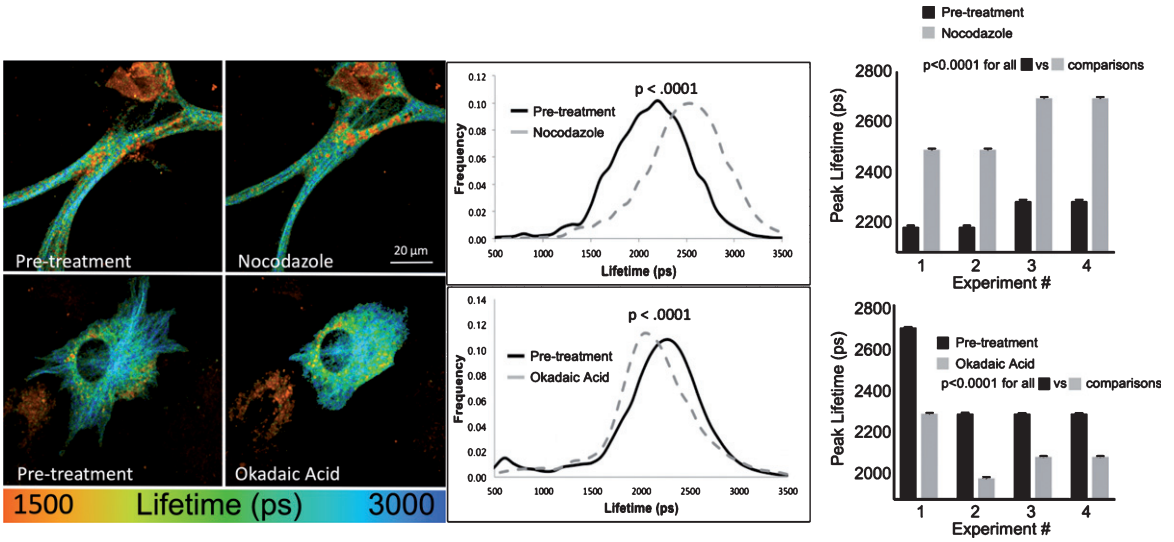

Fig. 4. Modulation of fluorescence lifetime by perturbation of microtubules and protein phosphorylation. CV-1 cells expressing Venus-Tau-Teal were treated on stage for 1 h with 1 μM nocodazole or okadaic acid. Middle panels show the results of a single experiment with distributions compared by the Kolmogorov-Smirnov test. Right panels show a summary of the peak lifetime results of four separate experiments.

determined by measuring the fluorescence intensity of the acceptor fluorochrome, Venus, using the 514 nm argon laser line to excite Venus without exciting Teal. For each pixel of a measured intensity, an E% was calculated and the data were binned into expression levels, as illustrated in Fig. 3. At low levels of biosensor expression (bins up to 500–750 arbitrary units of acceptor intensity), the increasing biosensor concentration did not have a significant effect on E%. At concentration ranges higher than this level, Venus-Tau-Teal yielded a concentration-dependent decrease in E%, indicating an intermolecular component to the signal.

In contrast, the Teal-Tau-Venus version of the biosensor did not yield a low Venus intensity range in which E% was independent of intensity. We therefore decided to use Venus-Tau-Teal for all further experiments. To minimize potential interference of intramolecular FRET caused by Venus-Tau-Teal aggregation, we also restricted our data collection for subsequent experiments to cells and regions of interest (ROIs) in which the Venus intensity was less than this determined range of intensity.

Venus-Tau-Teal is sensitive to microtubule loss and protein phosphatase inhibition

To test whether Venus-Tau-Teal responds to cellular perturbations, we first studied its properties under conditions in which microtubules were manipulated. A 1 h, 1 μM nocodazole treatment of CV-1 cells caused extensive microtubule depolymerization, a concomitant loss of Venus-Tau-Teal association with microtubules, and a shift toward longer Teal fluorescence lifetime (Fig. 4A–D). This lifetime increase is indicative of decreased FRET efficiency, implying that tau is predominantly in the paperclip/hairpin conformation when bound to microtubules and adopts a more open conformation when dissociated from microtubules. Treatment of CV-1 cells with the microtubule-stabilizing drug, taxol, which competes with tau for MT binding [32], yielded lesser effects on Teal lifetime (Supplementary Figure 2). In three of four experiments, taxol caused a small but statistically significant increase in Teal lifetime, which is consistent with a more open tau conformation.

We also tested the effects of overall protein phosphorylation on Venus-Tau-Teal lifetime. To do so we utilized okadaic acid (OA), a broad spectrum protein phosphatase inhibitor that preferentially inhibits protein phosphatase 2A and has been shown to cause several AD-like neuropathologies *in vitro* and *in vivo* [33]. Treatment of CV-1 cells for 1 h with 1 μM OA increased phosphorylation overall and specifically at p262 of Venus-Tau-Teal (Supplementary Figure 3), and caused a shortening of Teal fluorescence lifetime (Fig. 4). While this decrease in Teal lifetime might be due to phosphate accumulation on tau, for which 85 phosphorylation sites have been identified (http://cnr.iop.kcl.ac.uk/hangerlab/tautable),

increased phosphorylation of other proteins cannot be ignored as contributing factors.

Additionally, because phosphorylation of tau can induce its oligomerization [34], the possibility that the decrease in Teal lifetime induced by OA is due to intermolecular FRET, rather than increased intramolecular FRET should not be ignored. While our experimental design minimizes intermolecular FRET under basal conditions (see Fig. 3), local oligomerization might cause an increase in intermolecular FRET at low overall Venus-Tau-Teal concentrations that would otherwise detect predominantly intramolecular FRET. To shed further light on the fluorescence lifetime decrease caused by OA, CV-1 cells treated with OA were analyzed by western blotting with the tau oligomer antibodies, TOC1, TOMA-1, TTC-35, and TTC-99. None of those antibodies detected oligomeric tau either before or after exposing CV-1 cells to OA (data not shown). While these results imply that OA does not induce tau oligomerization, we cannot eliminate the possibilities that the fluorescent tags on the tau biosensor blocked binding of anti-tau oligomer antibodies to Venus-Tau-Teal that did oligomerize, or that the biosensors in OA-treated CV-1 cells formed specific types of oligomers that were not recognized by any of the anti-tau oligomer antibodies that we tested.

Venus-Tau-Teal responds to pathological oligomers of tau and Aβ

Extracellular tau oligomers have been found to cause aggregation of intracellular tau, accumulation of endogenous tau in the somatodendritic compartment, alteration of fast axonal transport, and synaptotoxicity [22, 35, 36]. Extracellular AβOs cause a separate set of adverse neuronal responses, such as impaired synaptic activity, ectopic neuronal cell cycle re-entry, which is a prelude to massive neuron death in AD [37], inhibition of nutrient-induced mitochondrial activity, and disruption of normal axon initial segment function [21, 38–44]. Because the new results presented here so far indicate that Venus-Tau-Teal can serve as a biosensor for conversions between the compact, paperclip/hairpin, and unfolded conformations of tau, we next tested if extracellular oligomers of tau or Aβ can alter Venus-Tau-Teal conformation.

After exposure of primary mouse cortical neurons to extracellular human 2N4R tau oligomers for 18 h, the Teal fluorescence lifetime of Venus-Tau-Teal shortened (Fig. 5), consistent with prior evidence that extracellular aggregated tau causes intracellular tau to aggregate [22, 35]. In contrast, when primary mouse cortical neurons were exposed to AβOs for 6 h, the Teal fluorescence lifetime of Venus-Tau-Teal increased (Fig. 6). This result indicates that AβOs induce tau unfolding from the paperclip/hairpin conformation.

DISCUSSION

Tau misfolding and aggregation underlie the pathogenesis of AD and non-Alzheimer's tauopathies, such as progressive supranuclear palsy, Pick's disease, Parkinson's disease, Huntington's disease, and many others. Several methods are well established for detecting aggregated tau, including binding of Congo red [45], and a variety of antibodies specific for oligomeric or fibrillar tau [46, 47], and PET imaging that can detect neurofibrillary tangles in live patients [48]. In contrast, methods to detect tau conformational changes that are thought to precede and promote tau aggregation are far more limited. Two monoclonal antibodies, Alz50 and MC-1, recognize similar discontinuous epitopes that comprise regions of tau near its N-terminal and within its microtubule-binding repeat region [16, 17]. The Alz50 and MC-1 epitopes are infrequently detected in normal brain, and Alz50 and MC-1 immunoreactivity are thought to represent a seminal step in the conversion of normal tau to pathogenic tau. The utility of Alz50 and MC-1 is limited, however, to examination of fixed cells and tissues.

Here we describe a new fluorescence-based biosensor, Venus-Tau-Teal, that can detect tau conformational changes in live cells. Venus-Tau-Teal can discriminate the tau paper-clip/hairpin conformation, in which the N- and C-termini are located in close proximity to each other and to the microtubule-binding repeat region [14, 15], from an unfolded conformation in which the tau N- and C-termini have dissociated. By expressing this biosensor in CV-1 cell fibroblasts and primary mouse cortical neurons, we gathered evidence that the paperclip/hairpin conformation predominates on microtubule-associated tau, and is sensitive to a variety of experimental perturbations.

This study represents a refinement of prior work that describes a similar biosensor, ECFP-Tau-EYFP, based on human 0N4R tau [19]. While our study focuses on a different isoform of the 6 that are

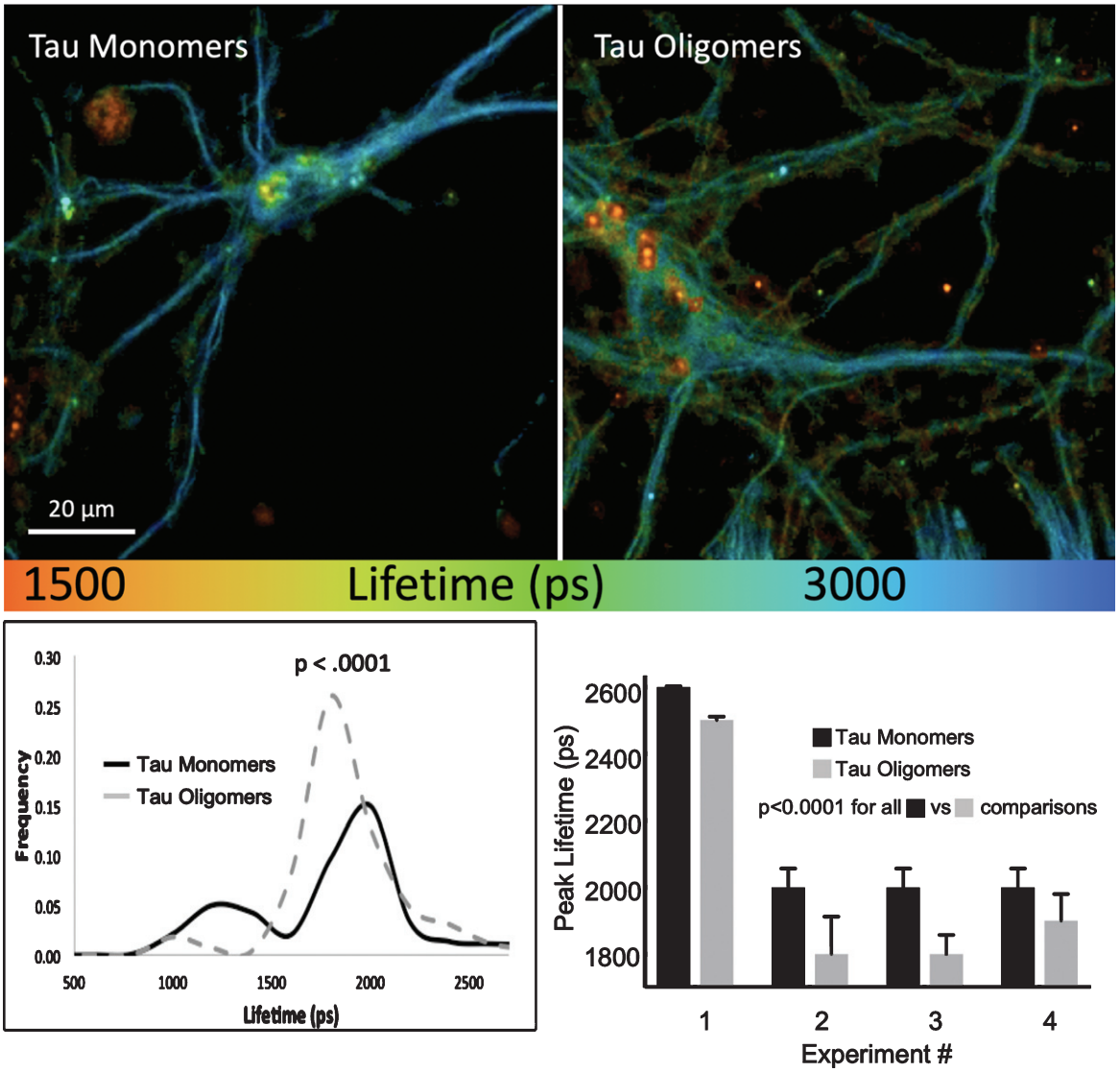

Fig. 5. Venus-Tau-Teal is sensitive to tau oligomers. Primary cortical mouse brain neurons were treated with human 2N4R tau monomers or oligomers at a total tau concentration of 250 nM for 18 h. Middle panels show the results of a single experiment with distributions compared by the Kolmogorov-Smirnov test. Right panels show a summary of the peak lifetime results of four separate experiments.

expressed in the central nervous system, there is precedence for tau isoform-specific toxicity [22, 49] and drug response [50]. Accordingly, further work with additional biosensors for other tau isoforms will be required to assess how widely the results reported here apply to isoforms other than 2N4R tau.

Besides being based on a different tau isoform, the Venus-Tau-Teal biosensor incorporates a superior FRET donor-acceptor pair [23, 24, 31] compared to ECFP-Tau-EYFP. Most critically, we defined, and exclusively relied on experimental conditions in which intramolecular FRET was minimally contaminated by intermolecular FRET and other possible complications caused by biosensor aggregation.

While most of the data presented here focused on the characterization of Venus-Tau-Teal (Figs. 1–4), our goal from the start was to develop a tau conformation biosensor that can discriminate normally folded from pathologically folded tau. We therefore included in the study experiments that monitored Venus-Tau-Teal responses to pathogenic extracellular oligomers made from tau or Aβ, each of which disrupts multiple aspects of neuronal homeostasis [21, 22, 36, 38–44, 51]. It is important to note that oligomers of tau and

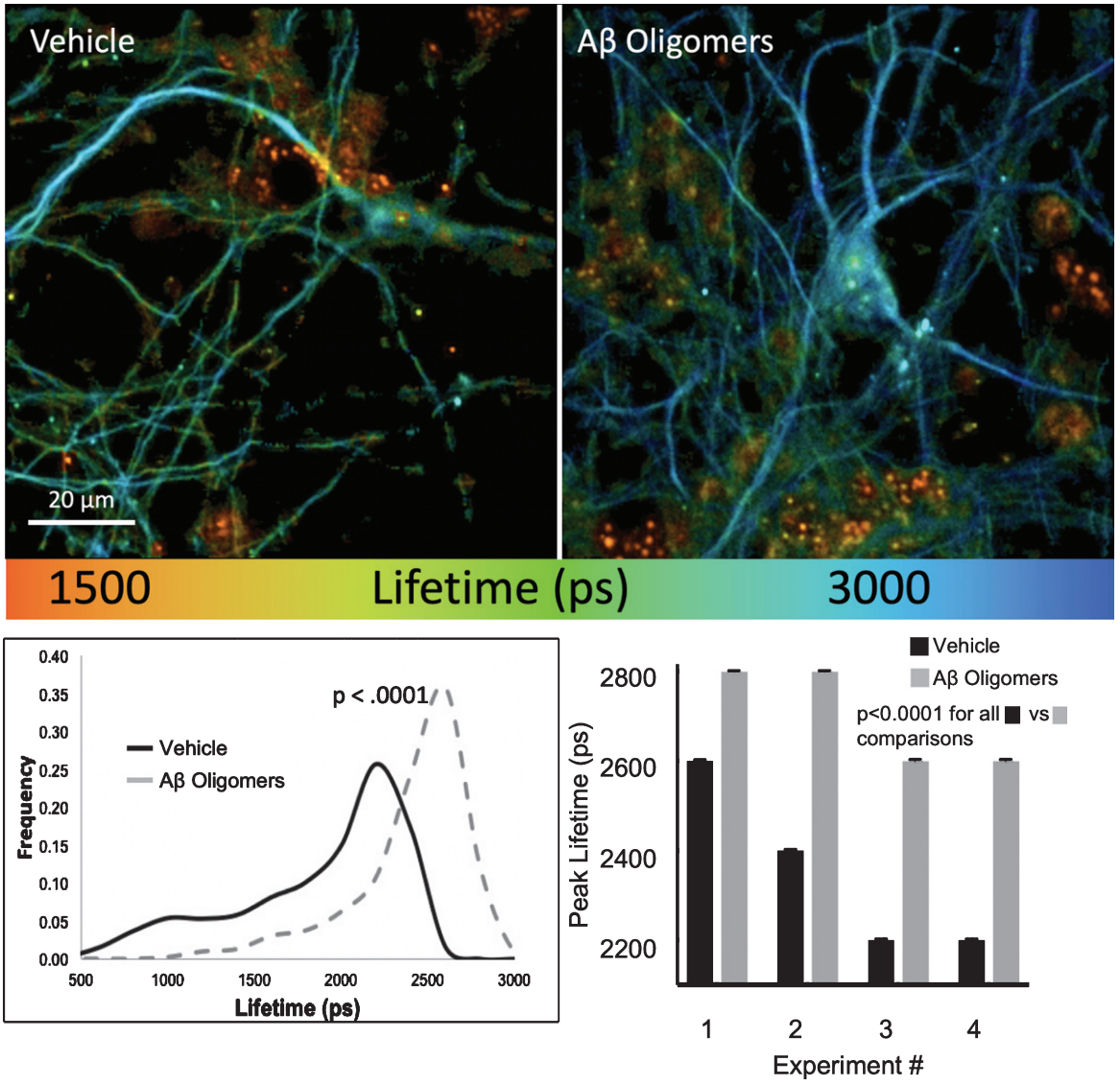

Fig. 6. Venus-Tau-Teal is sensitive to AβOs. Primary cortical mouse brain neurons were treated with vehicle or $A\beta_{1-42}$ oligomers at a total $A\beta_{1-42}$ concentration of approximately 1.5 µM for 6 h. The lower left panel shows the results of a single experiment with distributions compared by the Kolmogorov-Smirnov test. The lower right panel shows a summary of the peak lifetime results of four separate experiments.

Aβ are very heterogeneous in terms of their subunit composition and organization, and knowledge of their structures at the atomic resolution level is lacking. With this limitation in mind, in agreement with the work of Di Primio and colleagues [19], we found that extracellular tau oligomers cause increased biosensor FRET (Fig. 5), presumably due to intraneuronal tau aggregation [22, 35] in a manner that reinforces Teal-Venus proximity.

Extracellular AβOs caused the opposite response: lengthened Teal fluorescence lifetime of Venus-Tau-Teal, indicative of tau unfolding from the paperclip/hairpin conformation (Fig. 6). One mechanism by which this might occur involves site-specific tau phosphorylation by multiple protein kinases activated by AβOs. We have shown that AβOs induce ectopic neuronal cell cycle re-entry, which ironically leads to neuron death, by a mechanism that requires tau phosphor-ylation at Y18, S262, S409, and S416 by fyn, mTORC1 (probably indirectly through S6 kinase), protein kinase A and CaMKII, respectively [21, 44]. It is therefore possible that phosphorylation at some or all of those sites provokes the conformational change from compact and folded to unfolded.

Regardless of what the mechanism may be, the finding that AβOs cause tau unfolding emphasizes that biochemical effects of AβOs on tau, such as phosphorylation, are matched by changes in the physical structure of tau. It follows naturally that detection of molecular species that block or reduce AβO-induced tau unfolding might aid discovery of new diagnostic biomarkers and disease-modifying drugs for AD.

ACKNOWLEDGMENTS

This work was completed as part of the requirements for a Ph.D. degree for LKR. The authors would like to thank LKR's dissertation committee (Drs. Chris Deppmann, Sarah Siegrist, Bettina Winckler and Adrian Halme), Drs. John Lazo, Beth Sharlow and Murat Koseoglu, and the following past and current members of the Bloom lab—Drs. Erin Kodis, Shahzad Khan, Dora Bigler-Wang, Eric Swanson, Antonia Silva, and Andrés Norambuena; and Nutan Shivange, Merci Best and Victoria Sun—for their intellectual input throughout the course of this study. We also thank Dr. Raked Kayez of the University of Texas Medical Branch at Galveston for providing anti-tau oligomer antibodies. This work was supported by NIH/NIA grant RF1 AG051085 (GSB), the Owens Family Foundation (GSB), NIH/NIGMS training grant T32 GM008136, which provided 2 years of support for LRK, Alzheimer's Association Zenith Fellowship ZEN-16-363266 (GSB), the Cure Alzheimer's Fund (GSB, John Lazo and Beth Sharlow), and NIH/Office of the Director Funds award OD016446 to purchase the Zeiss 780 microscope that was used throughout these studies (AP).

Authors' disclosures available online (https://www.j-alz.com/manuscript-disclosures/19-0226r1).

SUPPLEMENTARY MATERIAL

The supplementary material is available in the electronic version of this article: http://dx.doi.org/10.3233/JAD-190226.

REFERENCES

[1] Barker WW, Luis CA, Kashuba A, Luis M, Harwood DG, Loewenstein D, Waters C, Jimison P, Shepherd E, Sevush S, Graff-Radford N, Newland D, Todd M, Miller B, Gold M, Heilman K, Doty L, Goodman I, Robinson B, Pearl G, Dickson D, Duara R (2002) Relative frequencies of Alzheimer disease, Lewy body, vascular and frontotemporal dementia, and hippocampal sclerosis in the State of Florida Brain Bank. *Alzheimer Dis Assoc Disord* **16**, 203-212.

[2] Drubin DG, Kirschner MW (1986) Tau protein function in living cells. *J Cell Biol* **103**, 2739-2746.

[3] Ebneth A, Godemann R, Stamer K, Illenberger S, Trinczek B, Mandelkow EM, Mandelkow E (1998) Overexpression of tau protein inhibits kinesin-dependent trafficking of vesicles, mitochondria, and endoplasmic reticulum: Implications for Alzheimer's disease. *J Cell Biol* **143**, 777-794.

[4] Dixit R, Ross JL, Goldman YE, Holzbaur ELF (2008) Differential regulation of dynein and kinesin motor proteins by tau. *Science* **319**, 1086-1089.

[5] Ksiezak-Reding H, Liu WK, Yen SH (1992) Phosphate analysis and dephosphorylation of modified tau associated with paired helical filaments. *Brain Res* **597**, 209-219.

[6] Sengupta A, Kabat J, Novak M, Wu Q, Grundke-Iqbal I, Iqbal K (1998) Phosphorylation of tau at both Thr 231 and Ser 262 is required for maximal inhibition of its binding to microtubules. *Arch Biochem Biophys* **357**, 299-309.

[7] Goedert M, Jakes R (1990) Expression of separate isoforms of human tau protein: Correlation with the tau pattern in brain and effects on tubulin polymerization. *EMBO J* **9**, 4225-4230.

[8] Brandt R, Lee G (1993) Functional organization of microtubule-associated protein tau. Identification of regions which affect microtubule growth, nucleation, and bundle formation *in vitro*. *J Biol Chem* **268**, 3414-3419.

[9] Bergen von M, Barghorn S, Li L, Marx A, Biernat J, Mandelkow EM, Mandelkow E (2001) Mutations of tau protein in frontotemporal dementia promote aggregation of paired helical filaments by enhancing local beta-structure. *J Biol Chem* **276**, 48165-48174.

[10] Schweers O, Schönbrunn-Hanebeck E, Marx A, Mandelkow E (1994) Structural studies of tau protein and Alzheimer paired helical filaments show no evidence for beta-structure. *J Biol Chem* **269**, 24290-24297.

[11] Mukrasch MD, Bibow S, Korukottu J, Jeganathan S, Biernat J, Griesinger C, Mandelkow E, Zweckstetter M (2009) Structural polymorphism of 441-residue tau at single residue resolution. *PLoS Biol* **7**, e34.

[12] Jeganathan S, Bergen von M, Mandelkow E-M, Mandelkow E (2008) The natively unfolded character of tau and its aggregation to Alzheimer-like paired helical filaments. *Biochemistry* **47**, 10526-10539.

[13] Bergen von M, Friedhoff P, Biernat J, Heberle J, Mandelkow EM, Mandelkow E (2000) Assembly of tau protein into Alzheimer paired helical filaments depends on a local sequence motif ((306)VQIVYK(311)) forming beta structure. *Proc Natl Acad Sci U S A* **97**, 5129-5134.

[14] Jeganathan S, Bergen von M, Brutlach H, Steinhoff H-J, Mandelkow E (2006) Global hairpin folding of tau in solution. *Biochemistry* **45**, 2283-2293.

[15] Horowitz PM, LaPointe N, Guillozet-Bongaarts AL, Berry RW, Binder LI (2006) N-terminal fragments of tau inhibit full-length tau polymerization *in vitro*. *Biochemistry* **45**, 12859-12866.

[16] Carmel G, Mager EM, Binder LI, Kuret J (1996) The structural basis of monoclonal antibody Alz50's selectivity for Alzheimer's disease pathology. *J Biol Chem* **271**, 32789-32795.

[17] Jicha GA, Bowser R, Kazam IG, Davies P (1997) Alz-50 and MC-1, a new monoclonal antibody raised to paired helical filaments, recognize conformational epitopes on recombinant tau. *J Neurosci Res* **48**, 128-132.

[18] Berry RW, Abraha A, Lagalwar S, LaPointe N, Gamblin TC, Cryns VL, Binder LI (2003) Inhibition of tau polymerization by its carboxy-terminal caspase cleavage fragment. *Biochemistry* **42**, 8325-8331.

[19] Di Primio C, Quercioli V, Siano G, Rovere M, Kovacech B, Novak M, Cattaneo A (2017) The distance between N and C termini of tau and of FTDP-17 mutants is modulated by microtubule interactions in living cells. *Front Mol Neurosci* **10**, 210.

[20] Bloom GS (2014) Amyloid-β and tau: The trigger and bullet in Alzheimer disease pathogenesis. *JAMA Neurol* **71**, 505-508.

[21] Seward ME, Swanson E, Norambuena A, Reimann A, Cochran JN, Li R, Roberson ED, Bloom GS (2013) Amyloid-β signals through tau to drive ectopic neuronal cell cycle re-entry in Alzheimer's disease. *J Cell Sci* **126**, 1278-1286.

[22] Swanson E, Breckenridge L, McMahon L, Som S, McConnell I, Bloom GS (2017) Extracellular tau oligomers induce invasion of endogenous tau into the somatodendritic compartment and axonal transport dysfunction. *J Alzheimers Dis* **58**, 803-820.

[23] Ai H-W, Henderson JN, Remington SJ, Campbell RE (2006) Directed evolution of a monomeric, bright and photostable version of Clavularia cyan fluorescent protein: Structural characterization and applications in fluorescence imaging. *Biochem J* **400**, 531-540.

[24] Nagai T, Ibata K, Park ES, Kubota M, Mikoshiba K, Miyawaki A (2002) A variant of yellow fluorescent protein with fast and efficient maturation for cell-biological applications. *Nat Biotechnol* **20**, 87-90.

[25] Porzig R, Singer D, Hoffmann R (2007) Epitope mapping of mAbs AT8 and Tau5 directed against hyperphosphorylated regions of the human tau protein. *Biochem Biophys Res Commun* **358**, 644-649.

[26] Patterson KR, Remmers C, Fu Y, Brooker S, Kanaan NM, Vana L, Ward S, Reyes JF, Philibert K, Glucksman MJ, Binder LI (2011) Characterization of prefibrillar tau oligomers *in vitro* and in Alzheimer disease. *J Biol Chem* **286**, 23063-23076.

[27] Elangovan M, Wallrabe H, Chen Y, Day RN, Barroso M, Periasamy A (2003) Characterization of one- and two-photon excitation fluorescence resonance energy transfer microscopy. *Methods* **29**, 58-73.

[28] Sun Y, Rombola C, Jyothikumar V, Periasamy A (2013) Förster resonance energy transfer microscopy and spectroscopy for localizing protein-protein interactions in living cells. *Cytometry A* **83**, 780-793.

[29] Sun Y, Day RN, Periasamy A (2011) Investigating protein-protein interactions in living cells using fluorescence lifetime imaging microscopy. *Nat Protoc* **6**, 1324-1340.

[30] Wallrabe H, Svindrych Z, Alam SR, Siller KH, Wang T, Kashatus D, Hu S, Periasamy A (2018) Segmented cell analyses to measure redox states of autofluorescent NAD(P)H, FAD & Trp in cancer cells by FLIM. *Sci Rep* **8**, 79.

[31] Day RN, Booker CF, Periasamy A (2008) Characterization of an improved donor fluorescent protein for Forster resonance energy transfer microscopy. *J Biomed Opt* **13**, 031203.

[32] Kar S, Fan J, Smith MJ, Goedert M, Amos LA (2003) Repeat motifs of tau bind to the insides of microtubules in the absence of taxol. *EMBO J* **22**, 70-77.

[33] Hamidi N, Nozad A, Sheikhkanloui Milan H, Amani M (2019) Okadaic acid attenuates short-term and long-term synaptic plasticity of hippocampal dentate gyrus neurons in rats. *Neurobiol Learn Mem* **158**, 24-31.

[34] Tepper K, Biernat J, Kumar S, Wegmann S, Timm T, Hübschmann S, Redecke L, Mandelkow E-M, Müller DJ, Mandelkow E (2014) Oligomer formation of tau protein hyperphosphorylated in cells. *J Biol Chem* **289**, 34389-34407.

[35] Frost B, Jacks RL, Diamond MI (2009) Propagation of tau misfolding from the outside to the inside of a cell. *J Biol Chem* **284**, 12845-12852.

[36] Kaniyappan S, Chandupatla RR, Mandelkow E-M, Mandelkow E (2017) Extracellular low-n oligomers of tau cause selective synaptotoxicity without affecting cell viability. *Alzheimers Dement* **13**, 1270-1291.

[37] Arendt T, Brückner MK, Mosch B, Lösche A (2010) Selective cell death of hyperploid neurons in Alzheimer's disease. *Am J Pathol* **177**, 15-20.

[38] Yang T, Li S, Xu H, Walsh DM, Selkoe DJ (2017) Large soluble oligomers of amyloid β-protein from Alzheimer brain are far less neuroactive than the smaller oligomers to which they dissociate. *J Neurosci* **37**, 152-163.

[39] Lei M, Xu H, Li Z, Wang Z, O'Malley TT, Zhang D, Walsh DM, Xu P, Selkoe DJ, Li S (2016) Soluble Aβ oligomers impair hippocampal LTP by disrupting glutamatergic/GABAergic balance. *Neurobiol Dis* **85**, 111-121.

[40] Walsh DM, Klyubin I, Fadeeva JV, Cullen WK, Anwyl R, Wolfe MS, Rowan MJ, Selkoe DJ (2002) Naturally secreted oligomers of amyloid beta protein potently inhibit hippocampal long-term potentiation *in vivo*. *Nature* **416**, 535-539.

[41] Varvel NH, Bhaskar K, Patil AR, Pimplikar SW, Herrup K, Lamb BT (2008) Abeta oligomers induce neuronal cell cycle events in Alzheimer's disease. *J Neurosci* **28**, 10786-10793.

[42] Norambuena A, Wallrabe H, Cao R, Wang DB, Silva A, Svindrych Z, Periasamy A, Hu S, Tanzi RE, Kim DY, Bloom GS (2018) A novel lysosome-to-mitochondria signaling pathway disrupted by amyloid-β oligomers. *EMBO J* **37**, e100241.

[43] Zempel H, Thies E, Mandelkow E, Mandelkow E-M (2010) Abeta oligomers cause localized Ca(2+) elevation, missorting of endogenous tau into dendrites, tau phosphorylation, and destruction of microtubules and spines. *J Neurosci* **30**, 11938-11950.

[44] Norambuena A, Wallrabe H, McMahon L, Silva A, Swanson E, Khan SS, Baerthlein D, Kodis E, Oddo S, Mandell JW, Bloom GS (2017) mTOR and neuronal cell cycle reentry: How impaired brain insulin signaling promotes Alzheimer's disease. *Alzheimers Dement* **13**, 152-167.

[45] Duff K, Kuret J, Congdon EE (2010) Disaggregation of tau as a therapeutic approach to tauopathies. *Curr Alzheimer Res* **7**, 235-240.

[46] Lasagna-Reeves CA, Castillo-Carranza DL, Sengupta U, Sarmiento J, Troncoso J, Jackson GR, Kayed R (2012) Identification of oligomers at early stages of tau aggregation in Alzheimer's disease. *FASEB J* **26**, 1946-1959.

[47] Castillo-Carranza DL, Sengupta U, Guerrero-Muñoz MJ, Lasagna-Reeves CA, Gerson JE, Singh G, Estes DM, Barrett ADT, Dineley KT, Jackson GR, Kayed R (2014) Passive immunization with Tau oligomer monoclonal antibody reverses tauopathy phenotypes without affecting hyperphosphorylated neurofibrillary tangles. *J Neurosci* **34**, 4260-4272.

[48] Park J-C, Han S-H, Yi D, Byun MS, Lee JH, Jang S, Ko K, Jeon SY, Lee Y-S, Kim YK, Lee DY, Mook-Jung I, KBASE Research Group (2019) Plasma tau/amyloid-β1–42

ratio predicts brain tau deposition and neurodegeneration in Alzheimer's disease. *Brain* **7**, 270.

[49] Liu C, Götz J (2013) Profiling murine tau with 0N, 1N and 2N isoform-specific antibodies in brain and peripheral organs reveals distinct subcellular localization, with the 1N isoform being enriched in the nucleus. *PLoS One* **8**, e84849.

[50] Ivashko-Pachima Y, Maor-Nof M, Gozes I (2019) NAP (davunetide) preferential interaction with dynamic 3-repeat Tau explains differential protection in selected tauopathies. *PLoS One* **14**, e0213666.

[51] Nussbaum JM, Schilling S, Cynis H, Silva A, Swanson E, Wangsanut T, Tayler K, Wiltgen B, Hatami A, Rönicke R, Reymann K, Hutter-Paier B, Alexandru A, Jagla W, Graubner S, Glabe CG, Demuth H-U, Nussbaum GB (2012) Prion-like behavior and tau-dependent cytotoxicity of β-amyloid oligomers seeded by pyroglutamylated β-amyloid. *Nature* **485**, 651-655.